Tissue Eng Regen Med (2023) 20(1):69–81
https://doi.org/10.1007/s13770-022-00506-9

Online ISSN 2212-5469

ORIGINAL ARTICLE

rhBMP-2-Conjugated Three-Dimensional-Printed Poly(L-lactide) Scaffold is an Effective Bone Substitute

Yu Ri Hong[1] · Tae-Ho Kim[1] · Kyeong-Hyeon Park[2,3] · Jumi Kang[4] · Kyueui Lee[4] · Eui Kyun Park[5] · Tae-Geon Kwon[6] · Jeong Ok Lim[1,2] · Chang-Wug Oh[3]

Received: 27 September 2022 / Revised: 27 October 2022 / Accepted: 30 October 2022 / Published online: 13 December 2022

Abstract

BACKGROUND: Bone growth factors, particularly bone morphogenic protein-2 (BMP-2), are required for effective treatment of significant bone loss. Despite the extensive development of bone substitutes, much remains to be desired for wider application in clinical settings. The currently available bone substitutes cannot sustain prolonged BMP-2 release and are inconvenient to use. In this study, we developed a ready-to-use bone substitute by sequential conjugation of BMP to a three-dimensional (3D) poly(L-lactide) (PLLA) scaffold using novel molecular adhesive materials that reduced the operation time and sustained prolonged BMP release.

METHODS: A 3D PLLA scaffold was printed and BMP-2 was conjugated with alginate-catechol and collagen. PLLA scaffolds were conjugated with different concentrations of BMP-2 and evaluated for bone regeneration *in vitro* and *in vivo* using a mouse calvarial model. The BMP-2 release kinetics were analyzed using ELISA. Histological analysis and micro-CT image analysis were performed to evaluate new bone formation.

RESULTS: The 3D structure of the PLLA scaffold had a pore size of 400 μm and grid thickness of 187–230 μm. BMP-2 was released in an initial burst, followed by a sustained release for 14 days. Released BMP-2 maintained osteoinductivity *in vitro* and *in vivo*. Micro-computed tomography and histological findings demonstrate that the PLLA scaffold conjugated with 2 μg/ml of BMP-2 induced optimal bone regeneration.

CONCLUSION: The 3D-printed PLLA scaffold conjugated with BMP-2 enhanced bone regeneration, demonstrating its potential as a novel bone substitute.

Keywords Bone regeneration · Bone morphogenetic protein 2 · Printing · Three-dimensional · PLLA scaffold

Yu Ri Hong and Tae-Ho Kim have contributed equally to this work as first authors.

✉ Jeong Ok Lim
jolim@knu.ac.kr

✉ Chang-Wug Oh
cwoh@knu.ac.kr

[1] Joint Institute for Regenerative Medicine, Kyungpook National University, Bio-Medical Research Institute, Kyungpook National University Hospital, Daegu 41940, Republic of Korea

[2] School of Medicine, Kyungpook National University, Daegu 41944, Republic of Korea

[3] Department of Orthopedic Surgery, School of Medicine, Kyungpook National University, Kyungpook National University Hospital, Daegu 41944, Republic of Korea

[4] Department of Chemistry and Green-Nano Materials Research Center, Kyungpook National University, Daegu 41566, Republic of Korea

[5] Department of Oral Pathology and Regenerative Medicine, School of Dentistry, Kyungpook National University, Daegu 41940, Republic of Korea

[6] Department of Oral and Maxillofacial Surgery, School of Dentistry, Kyungpook National University, Daegu 41940, Republic of Korea

1 Introduction

Generally, bone has the capacity to heal after minor damage. However, massive bone defects caused by traumatic injury, tumor resection, or congenital diseases cannot heal [1]. Current approaches for treating significant bone loss involve complex scaffolding biomaterials to fill the space and provide mechanical support with biologically functional molecules such as stem cells and bone growth proteins, including BMP-2 and BMP-7. TGF-β and PDGF are used for effective bone regeneration [2–5].

Among the various scaffold biomaterials, poly(L-lactide) (PLLA) is an ideal material for generating bone scaffolds owing to its high mechanical strength, comparable to that of natural bone, excellent biodegradability and biocompatibility, and ability to carry bioactive molecules such as bone growth factors [6–9]. The biomimetic 3D patterning of PLLA can be easily customized using 3D printing technology, thereby providing an ideal microenvironment for diverse signaling cues that influence cell fate and bone tissue regeneration [10–12].

Collagen, a key structural protein, is present in most tissues and organs, including the bones. Collagen type I is the main organic constituent of the bone extracellular matrix and has been used for decades as a supplementary protein in bone tissue engineering [13–15]. Therefore, it is important to provide collagen extraneously to bone defects to support bone formation.

BMP-2 is a potent growth factor that plays an important role in bone regeneration. Despite its valuable role in bone healing, its short half-life in the soluble state and the risk of tumor formation if overdosed limit its use [16, 17]. Therefore, controlled and localized delivery of bone growth-supporting supplementary proteins is highly desirable for safe and effective bone regeneration [18, 19]. However, the currently available methods for delivering these proteins are inefficient. For example, in conventional bone defect surgery, commercially available BMP-2 is physically mixed with a bone graft material (e.g., hydroxyapatite) prior to use. However, grafted proteins quickly dissolve in body fluids because of their inherent hydrophilicity, which affects bone regeneration [6]. In addition, this complex handling system increases the risk of surgical site infection.

Herein, we developed a ready-to-use bone substitute in which PLLA scaffolds and supplementary proteins are efficiently complexed in one block for easy and simple use, with the aim of enhancing bone regeneration. Strong conjugation of BMP-2 to the PLLA scaffold and collagen was achieved using a molecular binder, alginate-catechol. The bone regeneration capacity of this newly developed bone substitute was evaluated *in vitro* and *in vivo* using a mouse calvarial defect model.

2 Materials and methods

2.1 Materials

PLLA powder (Mol. wt. 102,000 g/mol) (Resomer L-206) was purchased from Boehringer Ingelheim Pharma KG (Boehringer Ingelheim, Ingelheim, Germany). Alginate and dopamine hydrochloride were purchased from Sigma-Aldrich (St. Louis, MO, USA) and Alfa Aesar (Haverhill, MA, USA), respectively. Type 1 collagen was purchased from Sigma-Aldrich (St. Louis, MO, USA). rhBMP-2 was purchased from CGBio (Novosis, CGBio, Seoul, Korea). The human BMP-2 ELISA kit and anti-Sp7/osterix were purchased from Abcam (Cambridge, UK).

2.2 Methods

2.2.1 Synthesis of alginate-catechol (Alg + Ca)

Alg + Ca was synthesized using the EDC(1-ethyl-3-(3′-dimethylaminopropyl)carbodiimide (EDC)/N-hydroxysuccinimide (NHS) coupling reaction, as described in a previous study [20]. Briefly, sodium alginate (1 g; ∼ 5 mmol; Sigma-Aldrich, A2033-100G) was dissolved in 100 mL of 0.1 M MES buffer (pH 5.2). EDC (5 mmol) and NHS (5 mmol) were then added dropwise to the alginate solution. After 5 min of nitrogen bubbling, dopamine hydrochloride (5 mmol) (Alfa Aesar, Ward Hill, MA, USA, A11136-25G) dissolved in 3 mL MES (0.1 M, pH 5.2) was added dropwise to the alginate/EDC/NHS solution. The reaction was allowed to proceed for 1 h at room temperature. After the reaction, the mixture was dialyzed against (3.5 kDa MWCO dialysis membrane) 5 L of deionized water (pH 6) and 20 g of NaCl for 3 days. Subsequently, the mixture was dialyzed against pure deionized water for 4 h and lyophilized for 3 days (Fig. 1). The as-synthesized alginate-catechol was confirmed using ^{1}H NMR spectroscopy (AVANCE III 500, Bruker, Billerica, MA, USA). The degree of substitution (DOS) of catechol in alginate was determined by measuring the absorbance at 280 nm (A_{280}) using a UV–Vis spectrophotometer (UV-1800, Shimadzu, Japan). Various concentrations (0.02–0.1 mg/mL) of dopamine hydrochloride were used to plot a standard curve for DOS calculation.

2.2.2 3D printing of the PLLA scaffold

A 3D printer (Invivo 4D2; ROKIT Healthcare, Seoul, Korea) was used to print the PLLA scaffold. The scaffold

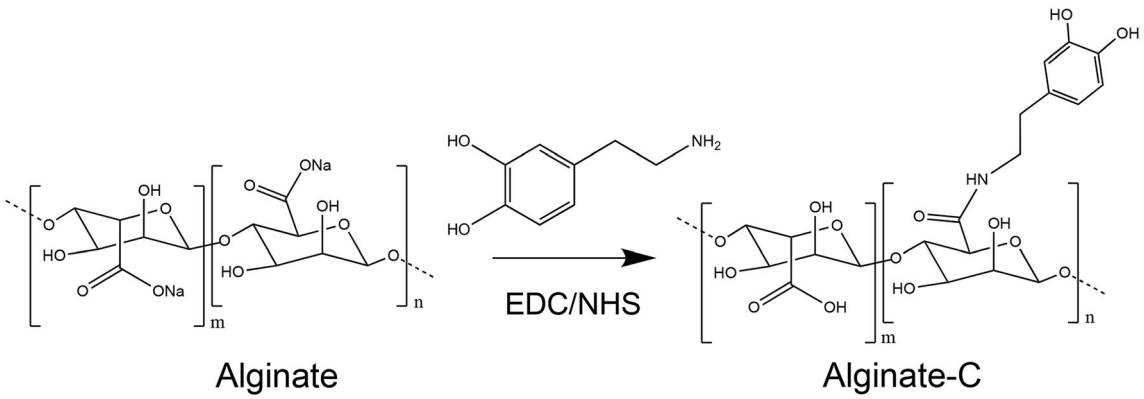

Fig. 1 Synthesis and chemical structure of alginate-catechol

was printed with a thickness of 1 mm and diameter of 5 mm. PLLA plastic was extruded at a fixed temperature of 200 °C. For all supports, the speed control was set at 3 mm/s, ejection pressure was 200–300 kPa, and support density was 15%. The porosity (%) was calculated using the following equation.

$$\text{Porosity } (\%) = \frac{\text{One pore volume} \times \text{Pore number in scaffold}}{\text{Total scaffold volume}} \times 100$$

2.2.3 Morphological analysis of 3D-printed PLLA by scanning electron microscopy (SEM)

The morphology of the 3D-printed PLLA scaffold was observed using SEM (Tescan MIRA3, Brno, Czech Republic) after coating with a thin film of gold (Quorum Q150T ES type, FEI, Hillsboro, OR, USA) at the Daegu Gyeongbuk Medical Innovation Foundation (DGMIF). The floor conditions were voltage, 10.0 kV; height, 9.1 mm; and magnification, 50×. The section conditions were voltage, 10.0 kV; height, 12.5 mm; magnification, 100×. The side-view conditions were voltage, 10.0 kV; height, 9.1 mm; magnification, 70×.

2.2.4 Sequential coating of rhBMP-2 and collagen on the PLLA scaffold surfaces via layer-by-layer assembly

The PLLA scaffold was coated with an Alg + Ca solution (0.5 mg/mL) on a rocker (50 rpm) at room temperature for 24 h. Next, the Alg + Ca–coated PLLA scaffold was coated with rhBMP-2 by immersion in low concentration (L group; 1 μg/mL) and high concentration (H group; 2 μg/mL) at 4 °C for 24 h. After BMP-2 coating, the scaffolds were coated with collagen via immersion in collagen type 1 (3 mg/mL).

Sequential coating of Alg + Ca, rhBMP-2, and collagen onto the PLLA scaffold was performed twice to form multiple layers of coating. The coated samples were then freeze-dried overnight. The coating procedure is illustrated in Fig. 2.

2.3 The kinetics of rhBMP-2 release from the 3D PLLA scaffold

The amount of rhBMP-2 released from the PLLA scaffolds was measured by ELISA. The PLLA scaffolds were placed in a siliconized microfuge tube containing 1 mL of 1 × phosphate buffered saline (PBS, pH 7.4) and incubated in a 37 °C water bath. The supernatant was collected daily for 14 days and stored at − 20 °C. At the end of the experiments, all collected samples were thawed and quantitatively analyzed using the Human BMP-2 ELISA Kit (ab277085, Abcam). The plates were read spectrophotometrically at 450 nm using a microplate reader (SpectraMax M2, Molecular Devices, San Jose, CA, USA). Cumulative releases were calculated as percentages of the total incorporated proteins.

2.4 *In vitro* study

2.4.1 Cytotoxicity and proliferation

Cell experiments were performed using the mouse preosteoblast MC3T3-E1 cell line or W-20-17 mouse stromal cell line purchased from the American Type Culture Collection (Manassas, VA, USA; CRL-2593). MC3T3-E1 and W-20-17 cells were cultured in α-minimum essential medium (α-MEM) without ascorbic acid (LM008-53; Welgene, Gyeongsan, Korea) and Dulbecco's modified Eagle's medium containing 4500 mg/mL D-glucose and 1500.00 mg/mL sodium bicarbonate (LM001-05; Welgene), respectively. *In vitro* cytotoxicity and proliferation tests were conducted using the scaffold extracts [21].

MC3T3-E1, the preosteoblast cell line, was used to test the cytotoxicity and cell proliferation in the presence of the

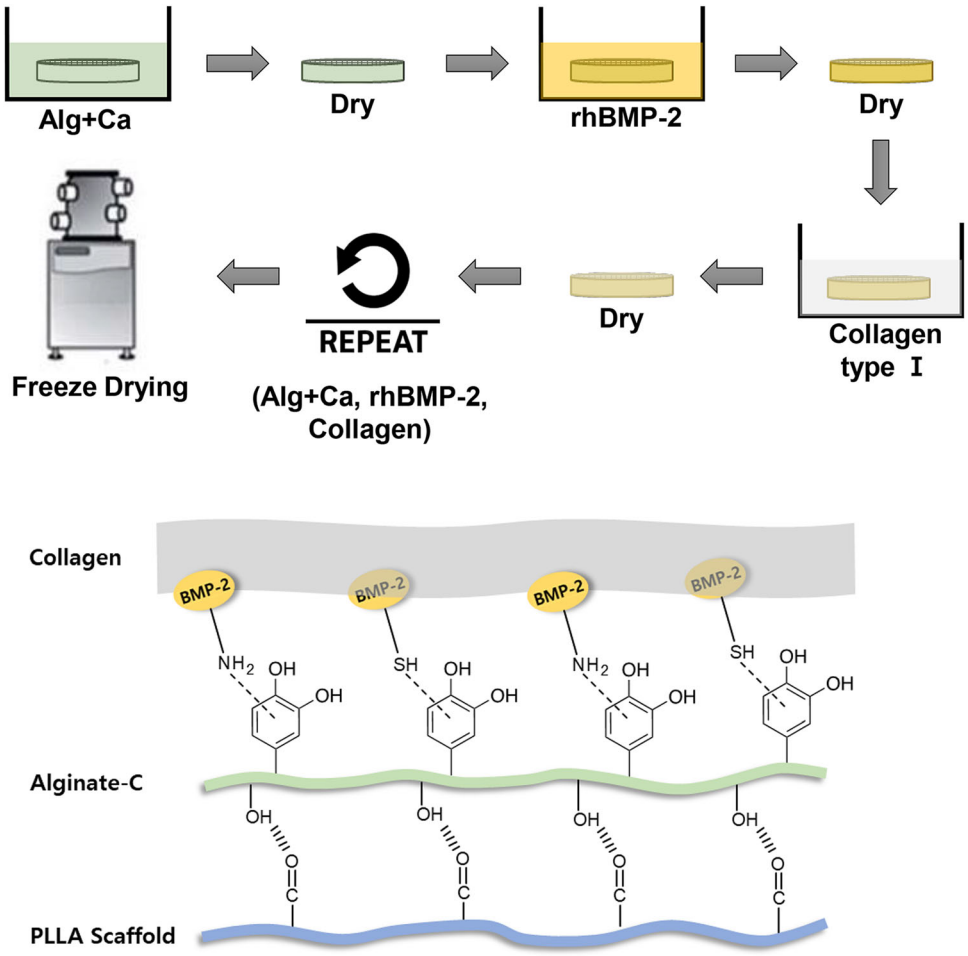

Fig. 2 Sequential coating of collagen and BMP-2 on the surface of the PLLA scaffold. Binding between PLLA, Alg + Ca, collagen, and BMP-2

PLLA scaffold. Briefly, MC3T3-E1 cells (7×10^3 cells/well) were seeded into 96-well plates. The next day, the media were replaced with α-MEM containing 10% (v/v) released media (PBS) from the 24 h BMP-2 release kinetic assays described in Sect. 2.3. After 48 h of culture, the original medium was carefully removed, 100 µL fresh medium plus 10 µL CCK-8 solution (Dojindo, Kumamoto, Japan) was added to each well, and the plates were incubated at 37 °C in a 5% CO_2 atmosphere for 2 h. The absorbance of each well was measured at 450 nm wavelength using a microplate reader (Spectra Max M2, Molecular Devices).

2.4.2 *Induction of osteoblast differentiation and alkaline phosphatase staining*

Alkaline phosphatase (ALP) expression is known to be increased in MC3T3-E1 osteoblastic progenitor cells and the W-20-17 mouse stromal cell line under conditions supporting osteocyte differentiation. MC3T3-E1 and W-20-17 cells were seeded into 96-well plates at densities of 1.6×10^4 and 1.3×10^4 cells per well, respectively. The next day, the culture medium was replaced with osteogenic media (OSM; α-MEM (or DMEM) containing 10 mM β-glycerol phosphate and 50 µg/mL L-ascorbic acid 2-phosphate), and the cells were incubated for 7 days. The medium released from the 24 h incubation was added at 10% (v/v) to the OSM medium. Cells treated with PLLA alone and pure BMP-2 (200 ng/mL) were used as negative and positive controls, respectively. Seven days after induction, the culture medium was aspirated and the cells were washed with physiological saline. The cells were lysed in 1% NP-40 by freeze-thawing (− 80 °C for 30 min, followed by incubation at 37 °C for 30 min). Absorbance at 405 nm was measured on a microplate reader using an ALP assay kit (Takara Bio, Shiga, Japan), according to the manufacturer's protocol. The measurements were normalized to the protein content estimated using the BCA protein assay (Pierce, Appleton, WI, USA). ALP activity was expressed in nanomoles of para-nitrophenol/min/mg protein, and ALP staining was performed using an ALP staining kit. (BCIP/NBT, Takara Bio).

2.5 *In vivo* study using a mouse calvarial defect model

2.5.1 Animal procedures

Animal experiments were performed in accordance with the guidelines approved by Kyungpook National University (approval no. 2021-0208). Male C57BL/6 mice (7-week-old; Hyochang Science, Daegu, Korea) were used as the critical-size calvarial defect model. Twenty-four C57BL/6 mice were randomly divided into six groups, housed in separate plastic cages, and allowed to adapt to the conditions of the animal house for seven days before surgery. Animals were anesthetized with an intraperitoneal (i.p.) injection of sodium pentobarbital (0.3 mL; 1%; 50 mg/kg) on a super clean bench. A sagittal skin incision was made over the scalp from the frontal bone to the occipital bone and the skin flap, including the periosteum. Full-thickness circular defects (5 mm diameter) were created in the left parietal bone using a 5 mm trephine bur (Saeshin, Daegu, Korea) with a slow dental handpiece (Saeshin Forte 400 s). After removal of the trephined calvarial disk, a disc-shaped scaffold specifically designed to fit the defects was transplanted into the defects. The transplanted discs were loaded with different doses of rhBMP-2 or without rhBMP-2. Empty calvarial defects were used as the negative controls (sham). The experimental groups included sham, PLLA only, PLLA + collagen (collagen-coated PLLA), and rhBMP-2 (low and high concentrations). Animals were housed at approximately 22 ± 1 °C under a 12-h light/dark cycle and had free access to tap water and a standard laboratory diet throughout the experiment.

2.5.2 Micro-CT imaging

At four weeks post-surgery, the skulls (n = 5) were fixed in 10% neutral buffered formalin at room temperature overnight and then stored in PBS at 4 °C until micro-CT. The specimens were scanned using a Skyscan 1275 Scanner (Bruker-microCT, Konich, Belgium) in high-resolution mode (X-ray voltage, 55 kV; anode current, 200 mA; aluminum filter, 0.5 mm; isotropic voxel size, 10 nm; exposure time, 100 ms). Scans were performed using the same calibration parameters and standardized reconstructions were performed using NRecon (Bruker). Datasets were analyzed using CTAn v1.11.10.0 (SkyScan) for the newly formed bone as well as the matching bone fragments in the defect. For the analysis, the region of interest is circled, and upper and lower thresholds of 160 and 60, respectively, are selected. The cylindrical volume of interest was defined as 5 mm in diameter and 1 mm in height, to include all new bone formations in the calvarial defect. Quantitative CT parameters were analyzed as the percentage volume of new bone formed (BV/TV) [22].

2.5.3 Histological evaluation based on hematoxylin and eosin (H&E) and Masson's trichrome (MT) stainings, and immunohistochemistry (IHC)

Twenty-four samples were demineralized with 10% ethylenediaminetetraacetic acid (EDTA) embedded in paraffin. The sections were stained with H&E and MT. Osterix expression in the calvaria was detected by IHC using anti-Sp7/osterix (Abcam, ab22552; 1:500) [23]. DAB horseradish peroxidase color development kit (Beyotime, Shanghai, China) was used to induce chromogenic reactions. All tissue sections were viewed using a Zeiss Axio Scan.Z1 digital slide scanner (Carl Zeiss, Oberkochen, Germany) with a 20 × objective. Bone regeneration and the area containing osteoblast cells were analyzed using ImageJ version 1.40 (National Institutes of Health, Bethesda, MD, USA).

2.6 Statistical analysis

Data are expressed as mean ± standard deviation and were analyzed using Student's *t*-test and one-way analysis of variance (ANOVA). A -test was used to analyze data between two independent groups, and one-way ANOVA was performed to analyze data among more than two independent groups. One-way ANOVA was followed by Tukey's test for post hoc analysis. The results were considered significant at $p < 0.05$.

3 Results

3.1 Morphology of 3D PLLA scaffolds

In this study, a porous PLLA scaffold was printed using the INVIVO bioprinter. The scaffold was fabricated with a diameter of 5 mm, thickness of 1 mm, pore size of 400 μm (Fig. 3A), and a grid thickness of 187–230 μm. These layers formed at regular intervals (Fig. 3B). A cross-sectional view of the structural morphology of the PLLA scaffold was obtained using SEM after sputter-coating the samples with gold (Fig. 3C). SEM images of the top (Fig. 3A), cross-sectional (Fig. 3B), and side (Fig. 3C) views are shown in Fig. 3. Our results show that a porous PLLA structure (82% porosity) was successfully formed.

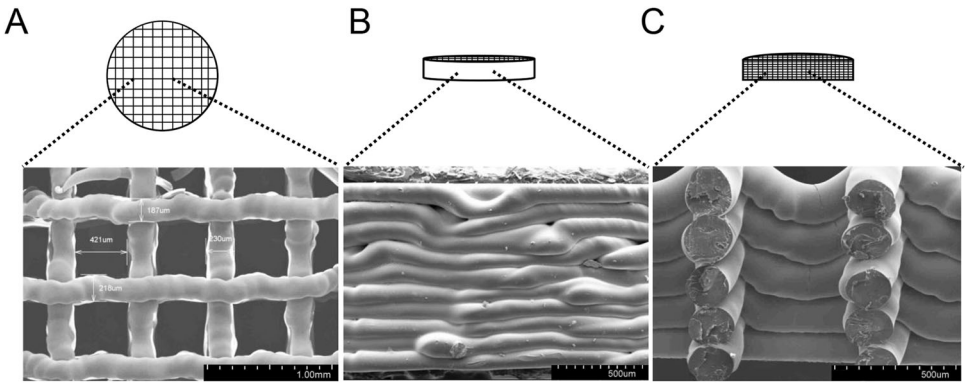

Fig. 3 SEM images of the PLLA scaffold. **A** Top view of the 3D PLLA scaffold. Scale bars, 1 mm; voltage, 10.0 kV; original magnification, 50×. **B** Side view of the 3D PLLA scaffold. Scale bars, 500 μm; voltage, 10.0 kV; original magnification, 70×. **C** Cross-sectional view of the 3D PLLA scaffold. Scale bars, 500 μm; voltage, 10.0 kV; original magnification, 100×

3.2 Release kinetics of rhBMP-2 from the 3D PLLA scaffold

We measured the amount of BMP-2 released from the scaffolds over 14 days. On the first day, approximately 488.25 ± 28.05 ng and 670.61 ± 62.49 ng was released from L and H groups, respectively (Fig. 4A). The cumulative amount released over 14 days was 617.15 ± 56.44 ng in L group and 1132.30 ± 125.78 ng in H group (Fig. 4B). Approximately 10 ng/day of rhBMP-2 was released from the L group, whereas 35 ng/day of rhBMP-2 was released from the H group. Both groups released rhBMP-2 in a sustained manner over 14 days, following an initial burst.

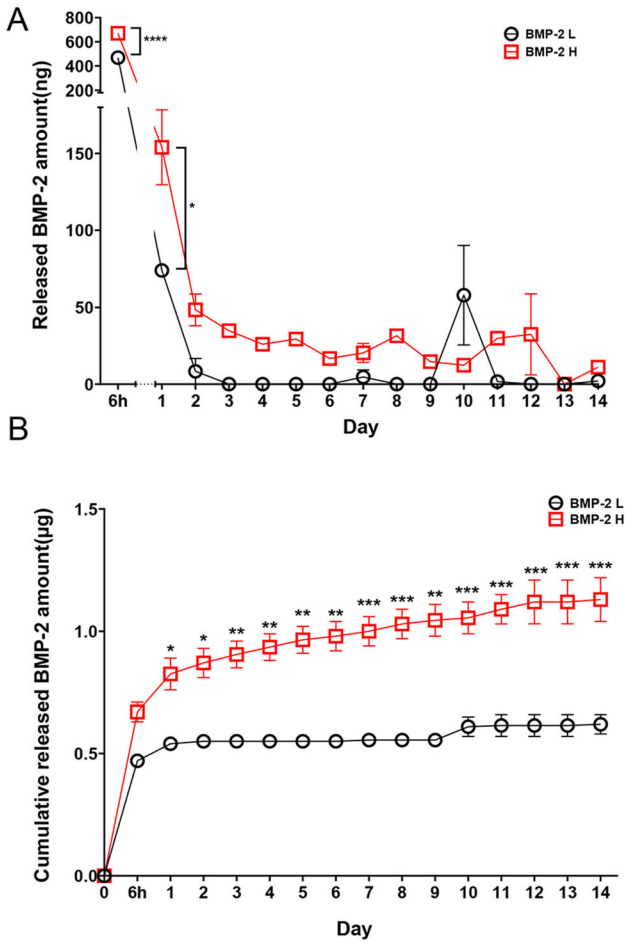

Fig. 4 Kinetic profile of BMP-2 released from scaffold. **A** Amount of BMP-2 released from scaffolds containing different BMP concentrations, **B** cumulative release of BMP-2 from scaffolds containing different BMP concentrations

3.3 Bioactivity of the released rhBMP-2 in the context of *in vitro* osteogenic differentiation

When performing BMP-2-release kinetic assays, the medium (PBS) was replaced daily. The samples are referred to as release media. To determine the cytotoxic effects of the PLLA/rhBMP-2 3D scaffolds, cytotoxicity tests were performed using the scaffold extracts prepared as described in Sect. 2.4. MC3T3-E1 cells were seeded at a density of 7×10^3 cells/mL in a 96-well plate, to which a normal medium containing 10% (v/v) scaffold eluate was added. The media released from the PLLA and PLLA/rhBMP-2 scaffolds did not show any cytotoxic effects or significant differences in cell proliferation (data not shown).

To determine the effect of media containing rhBMP-2 on osteoblast differentiation, MC3T3-E1 and W-20-17 cells were treated with the scaffold extracts (PLLA/rhBMP-2 with 48.8 ng/mL rhBMP-2) or rhBMP-2 (0.2 μg/mL; positive control). After 7 days of culture, ALP staining was performed to determine ALP activity. MC3T3-E1 and W-20-17 cells treated with BMP-2 or 0.2 μg/mL BMP-2 stained dark blue (BCIP/NBT reagent) owing to increased ALP activity (Fig. 5A). ALP activity assay also showed that the released rhBMP-2 maintained its activity (Fig. 5B). The results show that the treatment with released rhBMP-2 (48.8 ng/mL and 0.2 μg/mL) significantly promoted osteoblast differentiation compared to the treatment with the negative control release medium (PLLA only, Fig. 5B). Thus, the rhBMP-2 released from the scaffold retained its activity.

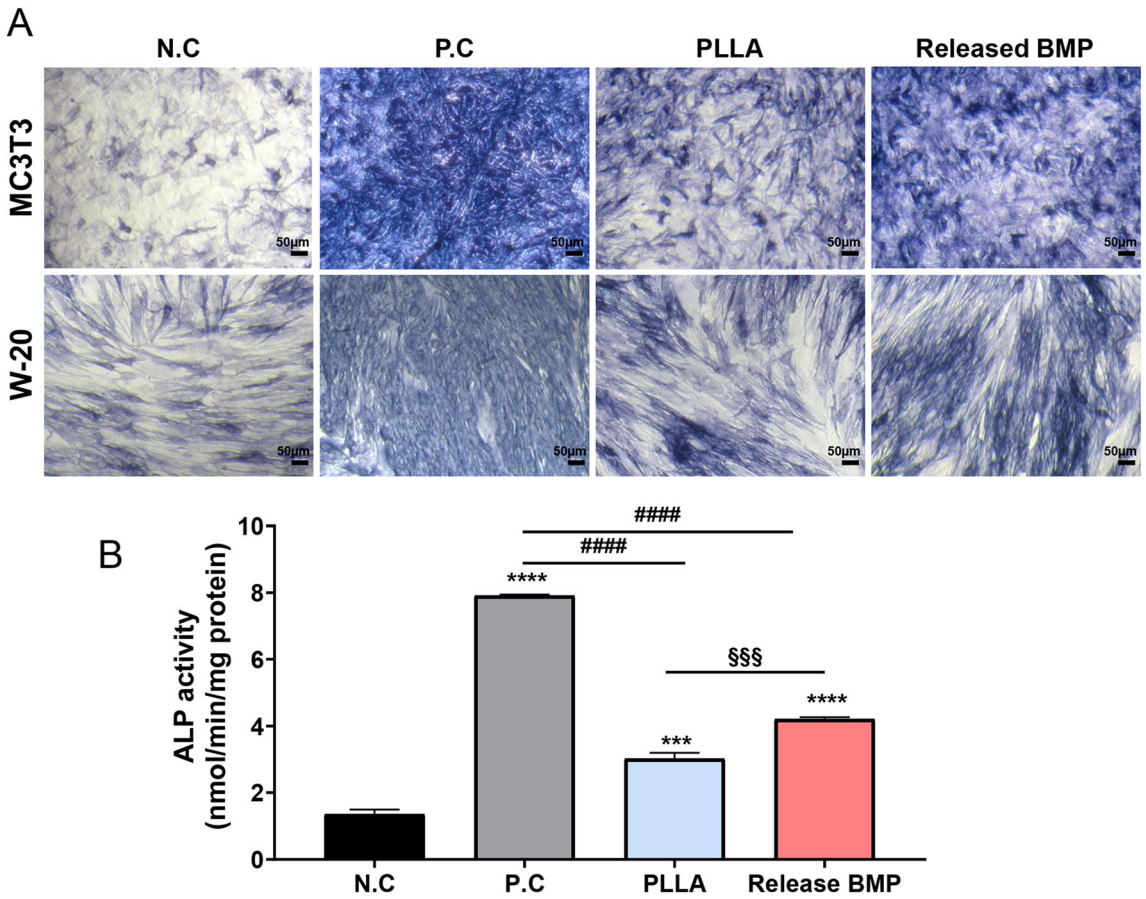

Fig. 5 Bioactivity analysis of BMP-2. Media released from the scaffold bound to high dose rhBMP-2 promoted the differentiation of primary osteoblasts. **A** Representative images of ALP staining showing that high doses of BMP-2 induced osteoblast differentiation. Scale bar, 50 μm. **B** Quantitative measurements of alkaline phosphatase (ALP) activity. Data represent the mean ± SD, N = 3. N.C, negative control; P.C, positive control; PLLA, PLLA only released media; Released BMP, high dose BMP-2 released media. Significant difference: $^{*}p < 0.05$; $^{**}p < 0.01$; $^{***}p < 0.001$; $^{****}p < 0.0001$

3.3.1 Micro-CT images of the newly regenerated bone

TO evaluate the bone regeneration capacity of the scaffold, a 5 mm diameter mouse calvarial model was prepared, and each scaffold was implanted. Animals in the sham group and those in which PLLA, PLLA + collagen, or rhBMP-2-coated scaffolds were transplanted were evaluated. Micro-CT images of samples obtained 4 weeks after skull implantation are shown in Fig. 6A. Almost no bone regeneration was observed in the sham group, and some bone regeneration was observed in the PLLA group. Bone regeneration was also observed in animals in the PLLA + collagen group. In contrast, in animals of the rhBMP-2 group, as the concentration increased, considerable bone regeneration was observed along the scaffold. In the sham group, bone formation was not observed with a bone volume of 0.02 ± 0.008 mm^3 (Fig. 6B). Compared with that in animals of the sham group, bone volume was 0.10 ± 0.05 mm^3 ($p = 0.0151$) and 0.18 ± 0.10 mm^3 ($p = 0.0036$) in animals of the PLLA and PLLA + collagen groups, respectively, indicating substantial bone regeneration. However, no significant differences were observed between the groups. Moreover, bone regeneration was observed in the group transplanted with the L group and H group scaffolds, with bone volumes of 0.41 ± 0.39 mm^3 ($p = 0.0351$) and 1.12 ± 0.26 mm^3, respectively ($p < 0.0001$) (Fig. 6B). Animals in the H group ($p < 0.0001$) exhibited markedly regenerated bone compared with those in the PLLA group. In addition, animals in the H group ($p < 0.0001$) exhibited significant bone regeneration compared with those in the PLLA + collagen group. Importantly, animals in the rhBMP-2 group exhibited bone regeneration in a BMP-2 dose-dependent manner (Fig. 6B).

3.4 Histological evaluation

Figure 7 shows the results of histological analysis of the samples retrieved 4 weeks after implantation. H&E staining did not reveal any tissue regeneration in animals in the

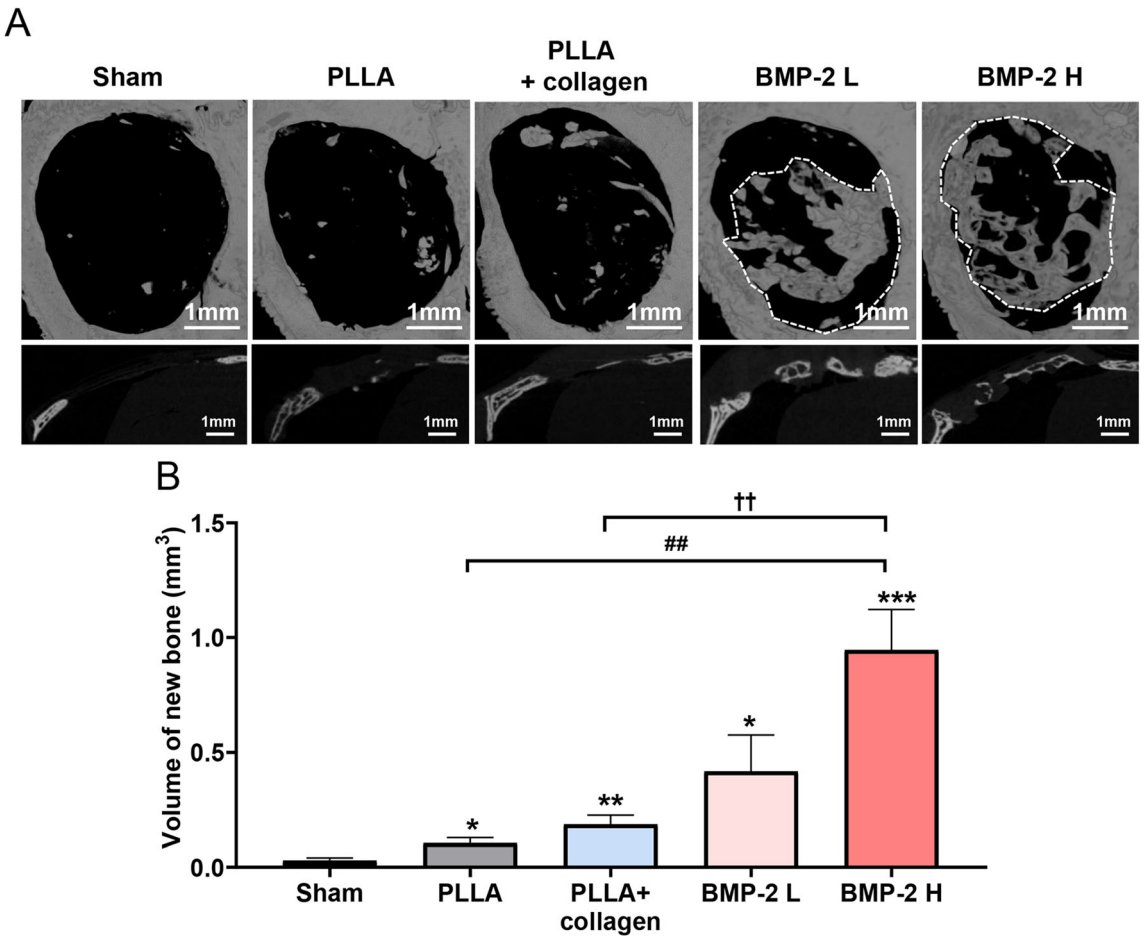

Fig. 6 Micro-CT analysis. **A** Three-dimensional reconstructed micro-CT of the calvarial bone defects at 4 weeks post-operation. Representative images of the calvarial bone defect in the sham, PLLA, PLLA + Collagen, BMP-2 L and BMP-2 H groups. Bone regeneration areas are indicated by dotted lines. Scale bar, 1 mm. **B** Volume of the newly regenerated bone at each time point. Data are expressed as mean ± SD (n = 4). Significant difference: $*p < 0.05$; $**p < 0.01$; $***p < 0.001$. Sham, sham control; PLLA, PLLA only; PLLA + Collagen, collagen-coated PLLA; BMP-2 L, PLLA containing 1 μg BMP-2; BMP-2 H, PLLA containing 2 μg rhBMP-2

sham group. Tissue regeneration was observed along the scaffold in animals in the PLLA group; however, the tissue thought to be bone did not regenerate. In contrast, in animals in the group in which the scaffold was coated only with collagen, regenerated tissue growth was observed around the existing bone. Although tissue regeneration was confirmed, it was not significant compared with that in the PLLA group. However, in animals from the groups implanted with the rhBMP-2-coated scaffold, regeneration of the bone tissue was visually confirmed (Fig. 7A). Complementary analysis of the same tissue was performed by MT staining (Fig. 7B), and the results revealed the absence of collagen or bone tissue in the sham group.

In animals in the PLLA group, limited tissue regeneration (2.48 ± 0.30 mm^2; $p = 0.0011$) was observed compared to that in animals in the sham group. Bone regeneration was clearly observed in animals of the PLLA + collagen group (3.09 ± 0.58 mm^2; $p < 0.0001$), compared to that in animals of the sham group. However, no difference was observed in the degree of bone regeneration in the PLLA group.

In contrast, animals transplanted with rhBMP-2-coated scaffolds exhibited significant bone regeneration compared with those in the sham group (Fig. 7C). In animals of the L group, the regenerated new bone areas were 3.68 ± 0.96 mm^2 ($p = 0.0003$) compared to those in the sham control, and the bone areas in animals of the H group were 4.49 ± 1.52 mm^2 ($p = 0.0002$). These results indicate that PLLA is capable of supporting bone regeneration on its own, and that PLLA and rhBMP-2 act synergistically to enable bone regeneration.

IHC of osteoblasts revealed the formation of new bone (Fig. 8). Osteoblast-positive cell area was 0.24 ± 0.56 mm^2 (Fig. 8A) in the sham group and 0.48 ± 0.68 mm^2 and 0.80 ± 1.38 mm^2, respectively in PLLA and PLLA + collagen groups. In addition, a synergistic effect of PLLA and rhBMP-2 was observed in the L group; these animals exhibited an osteoblast-positive

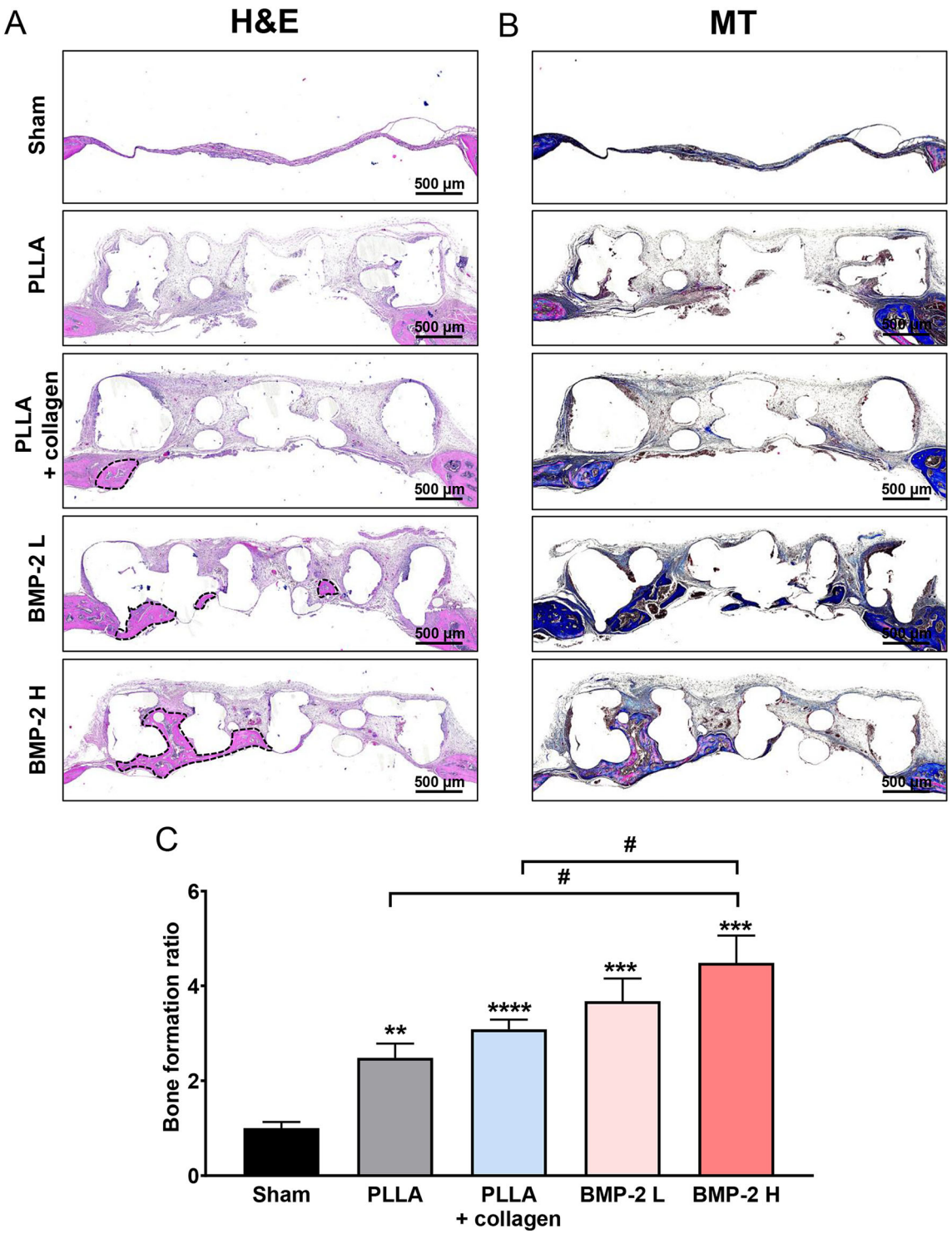

Fig. 7 Histomorphology analysis of the calvarial defects 4 weeks post-operation. **A** Representative H&E staining images of calvarial bone sections from animals of each group. **B** Representative MT staining images of calvarial bone sections from animals of each group. Calvarial bone sections were collected at post-operative week 4 and stained using H&E and MT. Representative sections with higher magnification from each group are shown. Scale bar, 500 μm. **C** Quantitative measurements were made using the MT-stained images. The new bone formation area in the calvarial defect site was measured, and the ratio of the bone matrix within the callus was calculated. Data are expressed as the mean ± SD (n = 4), and original magnification was 20×. The area of tissue regeneration is indicated by a black dotted line. $*p < 0.05$; $**p < 0.01$; $***p < 0.001$. Sham, sham control; PLLA, PLLA only; PLLA + Collagen, collagen-coated PLLA; BMP-2 L contained 1 μg rhBMP-2; BMP-2 H contained 2 μg rhBMP-2

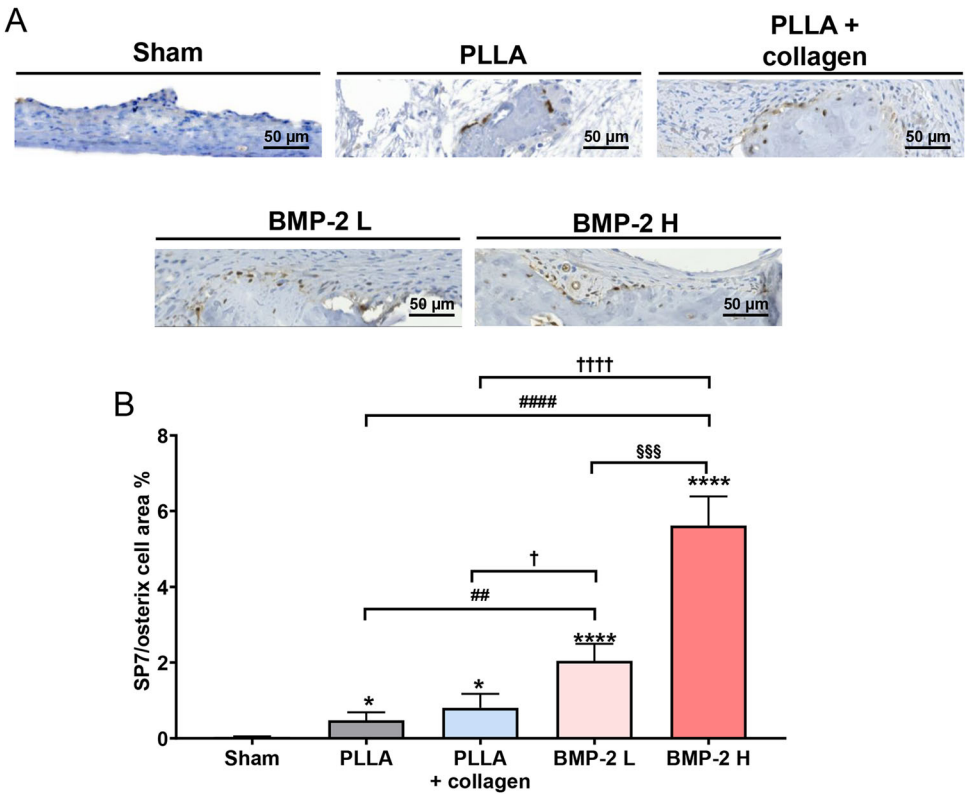

Fig. 8 IHC to evaluate the expression of osteoblast factor SP7/osterix in the calvarial defects 4 weeks post-operation. **A** The calvarial bone sections were evaluated for the expression of SP7/osterix. Representative sections with a higher magnification in each group are shown. Original magnification, 20×. Scale bar, 50 μm. **B** Osteoblast-positive cell area percent analysis. $^{*}p < 0.05$; $^{**}p < 0.01$; $^{***}p < 0.001$. Sham, sham control; PLLA, PLLA only; PLLA + Collagen, collagen-coated PLLA; BMP-2 L contained 1 μg rhBMP-2; BMP-2 H contained 2 μg rhBMP-2

area of 2.04 ± 1.69 mm^2 ($p = 0.05$), but this was not significantly different from that observed in the sham group. Animals in the H group (5.62 ± 2.32 mm^2; $p = 0.004$) had significantly increased osteoblast-positive areas compared to those in the sham group. Overall, excellent regeneration was observed in animals in the H group compared with that in the other groups (Fig. 8B).

4 Discussion

The use of biopolymer-based scaffolds that provide three-dimensional (3D) mechanical support to facilitate cell adhesion, migration, and differentiation *in vivo* has become an important strategy for bone regeneration [2–7]. Advanced 3D printing technology offers various advantages which enable fabrication of patient-specific bone grafts with precise pore size, geometry, and scaffold interconnectivity [24–26] that are better suited for use in clinical settings. The most commonly used synthetic and biodegradable bone regeneration scaffolds are poly(ε-caprolactone)(PCL), poly(glycolic acid) (PGA), poly(L-lactic acid) (PLLA), and their copolymers such as poly(lactic-co-glycolic acid)(PLGA) [7, 27]. Among these, PLLA is widely used in tissue engineering and regenerative medicine, particularly for bone regeneration [5]. PLLA is an FDA-approved polymer that exhibits good degradability, biocompatibility, and processability [21, 26]. Scaffolds meant for inducing bone regeneration should have mechanical properties comparable to those of bone (80–150 MPa). In this regard, PLLA, which exhibits a relatively high tensile strength (∼ 50 MPa) compared to other FDA-approved biopolymers such as PLGA (3–6 MPa), is an ideal candidate.

BMP-2, a widely used osteogenic growth factor, induces the osteogenic differentiation of multipotent mesenchymal cells and bone formation in both animals and humans [20, 21, 29]. Furthermore, bone regeneration can be enhanced by osteogenic growth factors, such as BMP-2, although it has a short half-life and requires an appropriate carrier (such as a matrix or scaffold) to maintain appropriate bioactivity once administered. In this study, we fabricated a 3D PLLA scaffold coated with collagen and BMP-2 to achieve efficient bone regeneration. Several polymeric delivery systems and scaffolds based on PLLA or PLGA have been prepared to deliver different payloads, ranging from nucleic acids and small drug molecules to large proteins, in a sustained-release manner to optimize payload function and activity [28].

Porosity is a key factor in scaffold design, and a 3D-printing system allows the precise control of scaffold porosity. The PLLA scaffold printed in this study exhibited an interconnected porous structure that provided an

increased area for effective molecular binding and cell proliferation [30].

For strong BMP-2 conjugation, alginate-catechol (which acts as a molecular binder) was synthesized and used as a functionalization tool for PLLA scaffolds. These two chemical interactions mainly contributed to the successful integration of BMP-2 under physiological pH (7.4) conditions. First, electrostatic interactions are generated between the carboxylic and hydroxyl groups of alginate (negatively charged) and the positively charged BMP-2 [31]. Second, a covalent bond was formed between the catechols of alginate-C and the nucleophilic group of BMP-2. This can be achieved by quinone formation during the spontaneous oxidation of catechol under slightly basic conditions; quinone acts as a strong electrophile, and thus, it can be conjugated with nucleophilic thiols and amines, which are ubiquitous in proteins [24].

BMP-2 is widely used to enhance bone regeneration, however, development of effective delivery system for sustainable release of BMP-2 is challenging due to weak binding of BMP-2 to substrates or scaffolding matrix. In this study, we used collagen for coating the BMP-2-conjugated PLLA scaffolds through utilizing its dual functions. Firstly, collagen type 1 is the main bone extracellular matrix and has been used for decades as a supplementary protein in bone tissue engineering. Therefore, it is important to provide collagen extraneously to bone defects to support bone formation. Secondly, as is well known, collagen has multiple functional sites to bind effectively with biological molecules such as BMP-2 through electrostatic interactions. Additional collagen coating to BMP-2 conjugated PLLA scaffolds resulted in a much more stable and stronger BMP-2 binding to PLLA scaffolds.

Tissue regenerative matrices designed to interact with cells must fulfill two conditions: they must not be cytotoxic and must support cell proliferation and differentiation [32]. In this study, the media released from PLLA/BMP-2 3D scaffolds were evaluated to determine whether these scaffolds were suitable for use in tissue regeneration. Our results show that the 10% (v/v) PLLA or PLLA/rhBMP-2 scaffold eluates did not present any cytotoxic effects on MC3T3-E1 cells.

ALP activity is a marker of osteogenic differentiation and plays an important role in mineral deposition. Treatment with BMP-2 (PLLA/BMP-2) or exogenous BMP-2 increased ALP content in MC3T3 and W20-17 cells, whereas treatment with PLLA alone (without BMP-2; negative control) did not have a significant effect on ALP content. This provided evidence that BMP-2 released from the PLLA/BMP-2 scaffolds was active and could induce osteogenic differentiation. These results are similar to those reported by other studies that demonstrated that BMP-2 facilitates the osteogenic differentiation of preosteoblasts or bone marrow stem cells by inducing ALP activity, thereby promoting mineralization, enhancing cell adherence, and mediating the expression and activation of certain associated osteogenic markers [25, 32–34].

To date, most studies on BMP-2 delivery for bone repair have employed a relatively high dose of BMP-2, which makes the treatment costly and raises safety concerns [35]. Previous studies have also investigated the use of lower doses in the range 0.5–5 μg [4, 36, 37]. In this study, PLLA/BMP-2 scaffolds were loaded with 1 μg and 2 μg of BMP-2. In the mouse calvarial model, scaffolds of PLLA-rhBMP-2 groups loaded with either low or high concentrations of rhBMP-2 induced significantly higher new bone formation than scaffolds without BMP-2, as observed by micro-CT analysis (Fig. 6). Even in the scaffolds containing low dose of BMP-2 (1 μg), there was an approximately 4.25-fold increase in new bone volume (0.85 mm^3) compared to the PLLA scaffold (0.2 mm^3) after 4 weeks of transplantation. In particular, scaffolds with a high concentration of BMP-2 (2 μg) showed an approximately tenfold (1.83 mm^3) increased in new bone formation compared to the PLLA control group, highlighting the osteoconductive characteristics of these scaffolds. Moreover, our scaffolds showed substantial bone regeneration *in vivo* compared with other studies that delivered high amounts of rhBMP-2 in a similar model [33]. Huang et al., reported that, in a mouse calvarial model, sandwich-type PLLA nanosheets loaded with 50 μg BMP-2 increased the volume of new bone by 1.5 mm^3 4 weeks after transplantation [37]. Similarly, only 10–20% bone repair was observed using this model when BMP-2 was delivered using hyaluronic acid hydrogel scaffolds [38]. Thus, we successfully developed an effective new bone substitute by combining the advantages of a 3D polymeric system and controlled release technology.

Although several BMP products have been used to promote bone healing, their clinical applications remain limited. As a common practice, the lyophilized form of BMP-2 is dissolved in solution and sprinkled onto a selected scaffold (either hydroxyapatite- or collagen sponge-based). The scaffold was then allowed to rest for 10–15 min to allow it to soak BMP-2. Since bleeding is inevitable at the site of a fracture or bone defect, irrigating or sucking the scaffold after implantation is not recommended. Solubilized BMP-2 may show biological effects only for the initial several hours after application. In this study, we were able to generate a ready-to-use product by conjugating rhBMP to a 3D PLLA scaffold that can reduce the operation time, decrease the risk of surgical site infection, and overcome the limitations and disadvantages of currently available products.

In conclusion, this newly developed hybrid scaffold offers a new therapeutic strategy as it allows a prolonged

and sustained release of BMP-2 at the site of a bone defect and enhances bone regeneration at the site of bone loss.

Acknowledgements This research was supported by the Korean Fund for Regenerative Medicine funded by the Ministry of Science and ICT and by the Ministry of Health and Welfare (21C0705L1-11). We thank Editage (www.editage.co.kr) for the English language editing.

Authors' contributions Jeong Ok Lim and Chang-Wug Oh conceived of the study, and edited the manuscript. Yu Ri Hong, Tae-Ho Kim, Jumi Kang, Kyueui Lee, Jeong Ok Lim and Chang-Wug Oh wrote the manuscript. Yu Ri Hong and Tae-Ho Kim performed experiments. Kyeong-Hyeon Park, Eui Kyun Park, and Tae-Geon Kwon analyzed data.

Declarations

Conflict of interest The authors have no conflicts of interest to declare.

Ethical statement Animal experiments were performed in accordance with the guidelines approved by Kyungpook National University (approval no. KNU-2021–0208; Daegu, Korea).

References

1. Bauer TW, Muschler GF. Bone graft materials. An overview of the basic science. Clin Orthop Relat Res. 2000;371:10–27.
2. Naveena N, Venugopal J, Rajeswari R, Sundarrajan S, Sridhar R, Shayanti M, et al. Biomimetic composites and stem cells interaction for bone and cartilage tissue regeneration. J Mater Chem. 2012;22:5239–53.
3. Zhang H, Migneco F, Lin CY, Hollister SJ. Chemically-conjugated bone morphogenetic protein-2 on three-dimensional polycaprolactone scaffolds stimulates osteogenic activity in bone marrow stromal cells. Tissue Eng Part A. 2010;16:3441–8.
4. Young S, Patel ZS, Kretlow JD, Murphy MB, Mountziaris PM, Baggett LS, et al. Dose effect of dual delivery of vascular endothelial growth factor and bone morphogenetic protein-2 on bone regeneration in a rat critical-size defect model. Tissue Eng Part A. 2009;15:2347–62.
5. Kim SS, Park MS, Jeon O, Choi CY, Kim BS. Poly (lactide-co-glycolide)/hydroxyapatite composite scaffolds for bone tissue engineering. Biomaterials. 2006;27:1399–409.
6. Cha M, Jin YZ, Park JW, Lee KM, Han SH, Choi BS, et al. Three-dimensional printed polylactic acid scaffold integrated with BMP-2 laden hydrogel for precise bone regeneration. Biomater Res. 2021;25:35.
7. Capuana E, Lopresti F, Ceraulo M, La Carrubba V. Poly-l-lactic acid (PLLA)-based biomaterials for regenerative medicine: a review on processing and applications. Polymers (Basel). 2022;14:1153.
8. Cho JW, Kim BS, Yeo DH, Lim EJ, Sakong S, Lim J, et al. 3D-printed, bioactive ceramic scaffold with rhBMP-2 in treating critical femoral bone defects in rabbits using the induced membrane technique. J Orthop Res. 2021;39:2671–80.
9. Chiesa-Estomba CM, Aiastui A, González-Fernández I, Hernáez-Moya R, Rodiño C, Delgado A, et al. Three-dimensional bioprinting scaffolding for nasal cartilage defects: a systematic review. Tissue Eng Regen Med. 2021;18:343–53.
10. Hassan MN, Yassin MA, Suliman S, Lie SA, Gjengedal H, Mustafa K. The bone regeneration capacity of 3D-printed templates in calvarial defect models: a systematic review and meta-analysis. Acta Biomater. 2019;91:1–23.
11. Zhang L, Yang G, Johnson BN, Jia X. Three-dimensional (3D) printed scaffold and material selection for bone repair. Acta Biomater. 2019;84:16–33.
12. Krishnan L, Priddy LB, Esancy C, Klosterhoff BS, Stevens HY, Tran L, et al. Delivery vehicle effects on bone regeneration and heterotopic ossification induced by high dose BMP-2. Acta Biomater. 2017;49:101–12.
13. Yiğiter Ö, Yorukoglu AC, Şentürk N, Dodurga Y, Demirkan AF. The effects of type I collagen on bone defects and gene expression changes for osteogenesis: in a rat model. J Cell Biochem. 2019;120:11525–30.
14. Bhakta G, Lim ZX, Rai B, Lin T, Hui JH, Prestwich GD, et al. The influence of collagen and hyaluronan matrices on the delivery and bioactivity of bone morphogenetic protein-2 and ectopic bone formation. Acta Biomater. 2013;9:9098–106.
15. Janjić K, Schädl B, Andrukhov O, Agis H. The response of gingiva monolayer, spheroid, and ex vivo tissue cultures to collagen membranes and bone substitute. J Tissue Eng Regen Med. 2020;14:1307–17.
16. Hu T, Liu L, Lam RWM, Toh SY, Abbah SA, Wang M, et al. Bone marrow mesenchymal stem cells with low dose bone morphogenetic protein 2 enhances scaffold-based spinal fusion in a porcine model. J Tissue Eng Regen Med. 2022;16:63–75.
17. Hollinger JO, Schmitt JM, Buck DC, Shannon R, Joh SP, Zegzula HD, et al. Recombinant human bone morphogenetic protein-2 and collagen for bone regeneration. J Biomed Mater Res. 1998;43:356–64.
18. Schliephake H, Weich HA, Dullin C, Gruber R, Frahse S. Mandibular bone repair by implantation of rhBMP-2 in a slow release carrier of polylactic acid—an experimental study in rats. Biomaterials. 2008;29:103–10.
19. Baheiraei N, Nourani MR, Mortazavi SMJ, Movahedin M, Eyni H, Bagheri F, et al. Development of a bioactive porous collagen/β-tricalcium phosphate bone graft assisting rapid vascularization for bone tissue engineering applications. J Biomed Mater Res A. 2018;106:73–85.
20. Kim K, Choi JH, Shin M. Mechanical stabilization of alginate hydrogel fiber and 3D constructs by mussel-inspired catechol modification. Polymers (Basel). 2021;13:892.
21. Wang MO, Etheridge JM, Thompson JA, Vorwald CE, Dean D, Fisher JP. Evaluation of the in vitro cytotoxicity of cross-linked biomaterials. Biomacromol. 2013;14:1321–9.
22. Lai L, Song H, Zhen J, Qiu Y, Liu X, Xu W, et al. Study on the bone morphogenetic protein 2 loaded synergistic hierarchical porous silk/carbon nanocage scaffold for the repair of bone defect. Mater Des. 2020;196:109105.
23. Wu Z, Bai J, Ge G, Wang T, Feng S, Ma Q, et al. Regulating macrophage polarization in high glucose microenvironment using lithium-modified bioglass-hydrogel for diabetic bone regeneration. Adv Healthc Mater. 2022;11:2200298.
24. Lee H, Rho J, Messersmith PB. Facile conjugation of biomolecules onto surfaces via mussel adhesive protein inspired coatings. Adv Mater. 2009;21:431–4.
25. Fung SL, Wu X, Maceren JP, Mao Y, Kohn J. In vitro evaluation of recombinant bone morphogenetic protein-2 bioactivity for regenerative medicine. Tissue Eng Part C Methods. 2019;25:553–9.
26. Liu S, Qin S, He M, Zhou D, Qin Q, Wang H. Current applications of poly (lactic acid) composites in tissue engineering and drug delivery. Compos B Eng. 2020;199:108238.
27. Sharma R, Kumar S, Gupta A, Dheer N, Jain P, Singh P, et al. An insight of nanomaterials in tissue engineering from fabrication to applications. Tissue Eng Regen Med. 2022;19:927–60.

28. Sun T, Zhang YS, Pang B, Hyun DC, Yang M, Xia Y. Engineered nanoparticles for drug delivery in cancer therapy. Nanomater Neoplasms. 2021;53:31–142.
29. Pelaez M, Susin C, Lee J, Fiorini T, Bisch FC, Dixon DR, et al. Effect of rh BMP-2 dose on bone formation/maturation in a rat critical-size calvarial defect model. J Clin Periodontol. 2014;41:827–36.
30. Abbasi N, Hamlet S, Love RM, Nguyen N-T. Porous scaffolds for bone regeneration. Adv Mater. 2020;5:1–9.
31. Wang Q, Wang M, Li P, Wang K, Fang L, Ren F, et al. The interaction of chitosan and BMP-2 tuned by deacetylation degree and pH value. J Biomed Mater Res A. 2019;107:769–79.
32. He W, Wei D, Zhang J, Huang X, He D, Liu B, et al. Novel bone repairing scaffold consisting of bone morphogenetic protein-2 and human beta defensin-3. J Biol Eng. 2021;15:5.
33. Li R, Ma Y, Zhang Y, Zhang M, Sun D. Potential of rhBMP-2 and dexamethasone-loaded Zein/PLLA scaffolds for enhanced in vitro osteogenesis of mesenchymal stem cells. Colloids Surf B Biointerfaces. 2018;169:384–94.
34. Sun J, Li J, Li C, Yu Y. Role of bone morphogenetic protein-2 in osteogenic differentiation of mesenchymal stem cells. Mol Med Rep. 2015;12:4230–7.
35. Bodde EW, Boerman OC, Russel FG, Mikos AG, Spauwen PH, Jansen JA. The kinetic and biological activity of different loaded rhBMP-2 calcium phosphate cement implants in rats. J Biomed Mater Res Part A. 2008;87:780–91.
36. Chung YI, Ahn KM, Jeon SH, Lee SY, Lee JH, Tae G. Enhanced bone regeneration with BMP-2 loaded functional nanoparticle–hydrogel complex. J Control Release. 2007;121:91–9.
37. Patterson J, Siew R, Herring SW, Lin AS, Guldberg R, Stayton PS. Hyaluronic acid hydrogels with controlled degradation properties for oriented bone regeneration. Biomaterials. 2010;31:6772–81.
38. Huang KC, Yano F, Murahashi Y, Takano S, Kitaura Y, Chang SH, et al. Sandwich-type PLLA-nanosheets loaded with BMP-2 induce bone regeneration in critical-sized mouse calvarial defects. Acta Biomater. 2017;59:12–20.